

Pseudo-Octahedral Schiff Base Nickel(II) Complexes: Does Single Oxidation Always Lead to the Nickel(III) Valence Tautomer?

Olaf Rotthaus,^[a] Vanessa Labet,^[a] Christian Philouze,^[a] Olivier Jarjayes,^{*[a]} and Fabrice Thomas^{*[a]}

Keywords: Phenoxy / Radicals / Nickel / Valence tautomerism / Schiff bases

With the aim of establishing correlations between the ligand structure and the oxidation site in nickel complexes from Schiff base ligands, five ligands and their nickel complexes have been synthesized. The prototypical asymmetric Schiff base ligand HL¹ contains both phenol and pyridine pendant arms with a pivotal imine nitrogen atom. Ligands HL^{2–5} differ from HL¹ by either their phenolate *para* substituent, the hybridization of the pivotal nitrogen atom, and/or the N-donor properties of the pyridine moiety. The five complexes [Ni(L^{1–5})₂] are obtained by treating the corresponding ligands with 0.5 equiv. of Ni(OAc)₂·4H₂O in the presence of NEt₃. X-ray crystal-structure diffraction studies as well as DFT calculations reveal that [Ni(L^{1–5})₂] involves a high-spin nickel(II) ion within a pseudo-octahedral geometry. The two ligands are arranged in a meridional fashion when the pivotal nitrogen atom is an imine [as in [Ni(L^{1–2})₂] and [Ni(L^{4–5})₂]], while the *fac* isomer is preferred in [Ni(L³)₂] (amino pivotal nitrogen atom). [Ni(L¹)₂] is characterized by an oxidation potential at –0.17 V vs. Fc⁺/Fc. The one-electron-oxidized species

[Ni(L¹)₂]⁺ exhibits an EPR signal at *g* = 2.21 attributed to a phenoxy radical that is antiferromagnetically coupled to a high-spin Ni^{II} ion. [Ni(L²)₂] differs from [Ni(L¹)₂] by the phenolate *para* substituent (a *tert*-butyl instead of the methoxy group) and exhibits an oxidation potential that is ca. 0.16 V higher. Compared to [Ni(L¹)₂]⁺ the cation [Ni(L²)₂]⁺ exhibits a SOMO that is more localized on the metal atom. The EPR and electrochemical signatures of [Ni(L³)₂]⁺ are similar to those of [Ni(L¹)₂]⁺, thus showing that an imino to amino substitution compensates for a methoxy to *tert*-butyl one. Replacement of the pyridine by a quinoline group in [Ni(L^{4–5})₂] makes the complexes slightly harder to oxidize. The EPR signatures of the cations [Ni(L^{4–5})₂]⁺ are roughly similar to those of the pyridine analogs [Ni(L^{1–2})₂]⁺. The oxidation site is thus not significantly affected by changes in the N-donor properties of the terminal imino nitrogen atom.

(© Wiley-VCH Verlag GmbH & Co. KGaA, 69451 Weinheim, Germany, 2008)

Introduction

Coordinated tyrosyl and phenoxy radicals have been the focus of increasing interest since the discovery of a Cu^{II}–tyrosyl radical entity in the active site of galactose oxidase ten years ago.^[1] As this enzyme constitutes a prototypical example of the synergy between a metal atom and a phenoxy radical to perform oxidation reactions, several biomimetic approaches to reproduce its active site have been developed by chemists. This has led to the characterization of a large number of copper(II) complexes involving coordinating redox-active phenolate groups.^[2] The localization of the oxidation site in these complexes could, however, lead to discrepancies as, in principle, electrons could be removed either from the metal center, leading to an M^{(*n*+1)⁺} closed-

shell ligand, or from the ligand, leading to an M^{*n*+} open-shell ligand. Practically, one-electron oxidation of these Cu^{II}–phenolate complexes has been shown to afford nearly all the time exclusively the M^{*n*+}–phenoxy valence tautomer.^[2] Recently, nickel complexes of pro-radicals,^[3] and especially pro-phenoxy ligands, have also emerged in the literature.^[4,5] In this case the ligand and metal redox-active orbitals are closer in energy. Therefore, while one-electron oxidation of the Cu^{II}–phenolate complexes affords M^{*n*+}–phenoxy species, one-electron oxidation of the Ni^{II}–phenolate complexes affords either the M^{(*n*+1)⁺}–phenolate or the M^{*n*+}–phenoxy valence tautomer.^[3–4] Such compounds are thus particularly useful to better understand the way in which nature could favor either a radical or a high-valent metal pathway to perform its oxidation reactions. They are not only interesting from a fundamental point of view but they are also valuable candidates for the design of molecular electronic devices and switches.^[6]

The oxidative behavior of low-spin nickel complexes of tetradentate Schiff bases has been investigated during the last few years. The electronic structure of these complexes in their one-electron-oxidized form has been elucidated only

[a] Département de Chimie Moléculaire, Chimie Inorganique Redox Biomimétique (CIRE), UMR-5250, Université Joseph Fourier
B. P. 53, 38041 Grenoble Cedex 9, France
Fax: +33-4-76514846
E-mail: Fabrice.Thomas@ujf-grenoble.fr

Supporting information for this article is available on the WWW under <http://www.eurjic.org/> or from the author.

recently: In CH_2Cl_2 they exhibit an Ni^{2+} -phenoxyl radical character with partial delocalization of the SOMO onto the metal orbitals,^[4b,4d-4j] the extent of which depends on the electronic properties of the phenolate *para* substituent.^[4j] In the presence of coordinating solvents such as methanol or pyridine, the square-planar low-spin Ni^{2+} -radical species are converted into pseudo-octahedral Ni^{3+} -phenolate complexes.^[4b,4c-4j,7]

These recent results would suggest that the oxidation site could be predicted or even controlled in these nickel complexes. In fact a direct correlation between the ligand structure and the oxidation site is still missing, and many questions remain unanswered: Is this behavior general for Schiff base nickel complexes? Does the initial nickel(II) geometry (and thus its spin state) affect the oxidation locus? What is the influence of the donor atoms?

In order to clarify this situation, we herein examine a unique series of pseudo-octahedral high-spin nickel complexes synthesized from tridentate Schiff base ligands. This series contrasts with previous ones as most of the one-electron-oxidized pseudo-octahedral Schiff base nickel complexes are low spin and involve a tetradentate Schiff base (pyridine or any bases and coordinating solvents are added to complete the coordination sphere). We show that complexes that belong to this series exhibit an unprecedented oxidative behavior. In addition, an extreme versatility in their oxidation locus makes them ideal candidates to develop a new logic of work that consists in counterbalancing the effect of one modification in the ligand structure by a second opposite one. We here demonstrate that by modifying a single parameter in the ligand both the electrochemical and EPR properties of the one-electron-oxidized nickel complex are affected. In contrast, modification of two independent parameters affords a one-electron-oxidized nickel complex that exhibits electrochemical and EPR signatures similar to those of the initial compound.

Results and Discussion

Design and Synthesis of the Ligands

Our strategy to obtain pseudo-octahedral Schiff base nickel complexes was based on the use of 2 equiv. of a tridentate ligand to coordinate a single metal ion.^[5,8-10] The prototypical asymmetric Schiff base ligand HL^1 (Figure 1) coordinates with two nitrogen atoms (from one pivotal imine and one terminal pyridine group) as well as an oxygen atom (from the redox-active phenolate group). Modifications realized on HL^1 concern the electronic properties of the phenol *para* substituent (HL^2), the hybridization of the pivotal nitrogen atom (HL^3), and the N-donor properties of the pyridine group (HL^{4-5}). We did not investigate the effect of hybridization of the terminal nitrogen atom as it has been reported in nickel complexes of related tridentate ligands that a terminal $\text{N}(\text{CH}_3)_2$ group was only poorly coordinating.^[5]

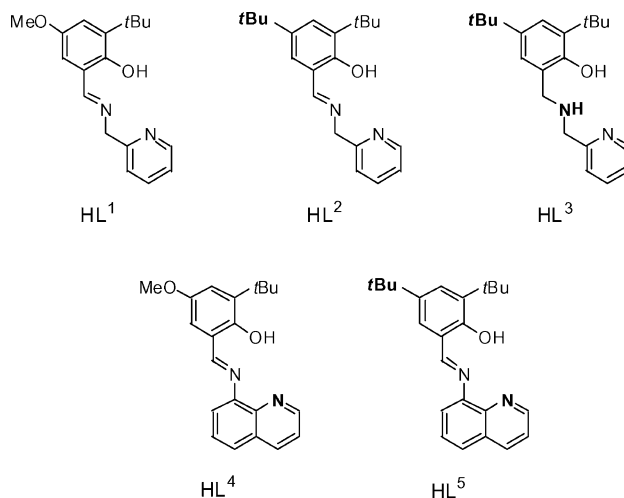


Figure 1. Chemical formulae of the ligands used in this study.

HL^1 was obtained by the treatment of 2-picolylamine with 2-*tert*-butyl-6-formyl-4-methoxyphenol. HL^2 ,^[8,9] HL^3 ,^[9,10] and HL^5 ^[8a] have been described previously. Treatment of 2-*tert*-butyl-6-formyl-4-methoxyphenol with 8-aminoquinoline affords HL^4 .

Structures of the Ni^{II} -Phenolate Complexes

The nickel(II) complexes $[\text{Ni}(\text{L}^{1-5})_2]$ have been obtained by mixing 2 equiv. of HL^{1-5} and 1 equiv. of $\text{Ni}(\text{OAc})_2 \cdot 4\text{H}_2\text{O}$ in the presence of NEt_3 . Single crystals of $[\text{Ni}(\text{L}^2)_2]$ and $[\text{Ni}(\text{L}^5)_2]$ were obtained by slow evaporation of methanol. Crystals of $[\text{Ni}(\text{L}^1)_2]$ could not be obtained by this method as the complex decomposes during solvent evaporation (one week). Nevertheless, crystals from a decomposition product $[\text{Ni}(\text{L}^6)]$ could be obtained.

The ORTEP diagrams of $[\text{Ni}(\text{L}^2)_2]$ and $[\text{Ni}(\text{L}^5)_2]$ are shown in Figure 2, and selected bond lengths and angles are listed in Table 1.

$[\text{Ni}(\text{L}^2)_2]$ consists of a nickel(II) ion in a pseudo-octahedral environment. The metal ion is surrounded by two deprotonated ligands that coordinate through nitrogen atoms from two pyridine rings [N(1) and N(3)] and two imine groups [N(2) and N(4)], as well as two oxygen atoms O(1) and O(2) from the phenolate groups. The two ligands are arranged in a meridional fashion, with a *cis* orientation of the phenolate moieties [the O(1)–Ni–O(2) angle is $97.5(1)^\circ$]. The imine nitrogen atoms are *trans* to one another with a N2–Ni–N4 angle of $177.68(8)^\circ$, whereas the pyridine nitrogen atoms are *cis* to one another with an N1–Ni–N3 angle of $92.84(7)^\circ$. The Ni–N_{pyridine} bond lengths Ni–N(1) and Ni–N(3) are 2.100(2) and 2.111(2) Å, respectively, the Ni–N_{imine} bond lengths Ni–N(2) and Ni–N(4) are 2.027(2) and 2.028(2) Å, respectively, whereas the Ni–O_{phenolate} bond lengths Ni–O(1) and Ni–O(2) are 2.021(2) and 2.003(2) Å, respectively. These bond lengths are typical for complexes involving a high-spin nickel(II) ion. This spin state is also in agreement with the pseudo-octahedral geometry generally adopted by the nickel ion in this electronic configuration.

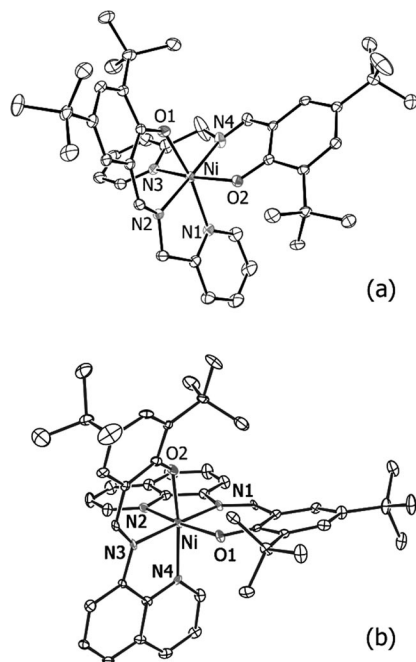


Figure 2. X-ray crystal structure of $[\text{Ni}(\text{L}^2)_2]$ (a) and $[\text{Ni}(\text{L}^5)_2]$ (b) shown with 30% thermal ellipsoids. H atoms are omitted for clarity. The crystal cell of $[\text{Ni}(\text{L}^2)_2]$ contains two independent complexes (only one complex is shown and was chosen arbitrarily).

The crystal cell of $[\text{Ni}(\text{L}^5)_2]$ contains two independent complexes. The geometry was found to be very similar to that adopted for $[\text{Ni}(\text{L}^2)_2]$. The phenolate oxygen atoms are *cis* to one another with $\text{O}(1)\text{--Ni}(1)\text{--O}(2)$ and $\text{O}(3)\text{--Ni}(2)\text{--O}(4)$ angles of $88.5(1)$ and $88.0(1)^\circ$, respectively, the imine nitrogen atoms are *trans* to one another with $\text{N}(1)\text{--Ni}(1)\text{--N}(3)$ and $\text{N}(5)\text{--Ni}(2)\text{--N}(7)$ angles of $173.3(2)$ and $171.6(2)^\circ$, respectively, whereas the quinoline nitrogen atoms are *cis* to one another with $\text{N}(2)\text{--Ni}(1)\text{--N}(4)$ and $\text{N}(6)\text{--Ni}(2)\text{--N}(8)$ angles of $88.8(2)$ and $88.8(2)^\circ$, respectively. The $\text{Ni}\text{--N}_{\text{imine}}$ bond lengths $\text{Ni}(1)\text{--N}(1)$, $\text{Ni}(1)\text{--N}(3)$, $\text{Ni}(2)\text{--N}(5)$, and $\text{Ni}(2)\text{--N}(7)$ are $2.019(4)$, $2.028(4)$, $2.017(4)$, and $2.003(4)$ Å, respectively, whereas the $\text{Ni}\text{--O}_{\text{phenolate}}$ bond lengths $\text{Ni}(1)\text{--O}(1)$, $\text{Ni}(1)\text{--O}(2)$, $\text{Ni}(2)\text{--O}(3)$, and $\text{Ni}(2)\text{--O}(4)$ are $2.003(4)$, $2.019(3)$, $2.008(4)$, and $2.032(3)$ Å, respectively. They are thus close to those obtained for $[\text{Ni}(\text{L}^2)_2]$. As expected, the $\text{Ni}\text{--N}_{\text{quinoline}}$ bonds $\text{Ni}(1)\text{--N}(2)$, $\text{Ni}(1)\text{--N}(4)$, $\text{Ni}(2)\text{--N}(6)$, and $\text{Ni}(2)\text{--N}(8)$ are longer, with values of $2.096(4)$, $2.118(4)$, $2.109(4)$, and $2.120(4)$ Å, respectively. The $\text{Ni}\text{--N}_{\text{quinoline}}$ bond lengths in $[\text{Ni}(\text{L}^5)_2]$ are quite similar to the $\text{Ni}\text{--N}_{\text{pyridine}}$ bond lengths obtained for $[\text{Ni}(\text{L}^2)_2]$. They are also much shorter than the $\text{Ni}\text{--N}_{\text{amine}}$ bond length reported for a pseudo-octahedral nickel(II) complex of a tridentate Schiff base ligand involving a terminal $\text{N}(\text{CH}_3)_2$ nitrogen atom ($2.318\text{--}2.463$ Å).^[5] The $\text{Ni}\text{--N}_{\text{terminal}}$ bond, and consequently the octahedral ligand field, is thus much stronger when the terminal N-donor is a pyridine or a quinoline group.

The X-ray crystal structure of $[\text{Ni}(\text{L}^6)]$ {complex resulting from the decomposition of $[\text{Ni}(\text{L}^1)_2]$ } differs significantly from the former two complexes (Figure 3). The nick-

Table 1. Selected bond lengths [Å] and angles [$^\circ$] for $[\text{Ni}(\text{L}^2)_2]$, $[\text{Ni}(\text{L}^5)_2]$, and $[\text{Ni}(\text{L}^6)]$.

	$[\text{Ni}(\text{L}^2)_2]$	$[\text{Ni}(\text{L}^5)_2]$	$[\text{Ni}(\text{L}^6)]$
$\text{Ni}(1)\text{--O}(1)$	2.021(2)	2.003(4)	1.823(1)
$\text{Ni}(1)\text{--O}(2)$	2.003(2)	2.019(3)	
$\text{Ni}(1)\text{--N}(1)$	2.100(2)	2.019(1)	1.822(1)
$\text{Ni}(1)\text{--N}(2)$	2.027(2)	2.096(4)	1.821(1)
$\text{Ni}(1)\text{--N}(3)$	2.111(2)	2.028(4)	1.917(1)
$\text{Ni}(1)\text{--N}(4)$	2.028(2)	2.118(4)	
$\text{Ni}(2)\text{--O}(3)$		2.008(4)	
$\text{Ni}(2)\text{--O}(4)$		2.032(3)	
$\text{Ni}(2)\text{--N}(5)$		2.017(4)	
$\text{Ni}(2)\text{--N}(6)$		2.109(4)	
$\text{Ni}(2)\text{--N}(7)$		2.003(4)	
$\text{Ni}(2)\text{--N}(8)$		2.120(4)	
$\text{O}(1)\text{--Ni}(1)\text{--O}(2)$	97.45(6)	88.5(1)	
$\text{O}(1)\text{--Ni}(1)\text{--N}(1)$	166.93(6)	90.6(2)	96.60(6)
$\text{O}(1)\text{--Ni}(1)\text{--N}(2)$	88.42(7)	170.9(2)	176.49(6)
$\text{O}(1)\text{--Ni}(1)\text{--N}(3)$	84.87(6)	94.1(2)	94.77(6)
$\text{O}(1)\text{--Ni}(1)\text{--N}(4)$	91.08(6)	92.8(2)	
$\text{O}(2)\text{--Ni}(1)\text{--N}(1)$	87.42(7)	93.8(2)	
$\text{O}(2)\text{--Ni}(1)\text{--N}(2)$	88.83(8)	91.3(2)	
$\text{O}(2)\text{--Ni}(1)\text{--N}(3)$	168.15(6)	91.0(1)	
$\text{O}(2)\text{--Ni}(1)\text{--N}(4)$	88.99(6)	170.8(2)	
$\text{N}(1)\text{--Ni}(1)\text{--N}(2)$	79.53(7)	80.3(2)	85.42(6)
$\text{N}(1)\text{--Ni}(1)\text{--N}(3)$	92.84(7)	173.3(2)	167.40(6)
$\text{N}(1)\text{--Ni}(1)\text{--N}(4)$	101.16(7)	95.3(2)	
$\text{N}(2)\text{--Ni}(1)\text{--N}(3)$	102.88(8)	94.9(2)	83.51(6)
$\text{N}(2)\text{--Ni}(1)\text{--N}(4)$	177.68(8)	88.8(2)	
$\text{N}(3)\text{--Ni}(1)\text{--N}(4)$	79.33(6)	79.8(2)	
$\text{O}(3)\text{--Ni}(2)\text{--O}(4)$		88.0(1)	
$\text{O}(3)\text{--Ni}(2)\text{--N}(5)$		91.0(2)	
$\text{O}(3)\text{--Ni}(2)\text{--N}(6)$		171.1(2)	
$\text{O}(3)\text{--Ni}(2)\text{--N}(7)$		94.4(2)	
$\text{O}(3)\text{--Ni}(2)\text{--N}(8)$		91.2(2)	
$\text{O}(4)\text{--Ni}(2)\text{--N}(5)$		96.0(2)	
$\text{O}(4)\text{--Ni}(2)\text{--N}(6)$		93.5(2)	
$\text{O}(4)\text{--Ni}(2)\text{--N}(7)$		90.6(2)	
$\text{O}(4)\text{--Ni}(2)\text{--N}(8)$		170.0(2)	
$\text{N}(5)\text{--Ni}(2)\text{--N}(6)$		80.1(2)	
$\text{N}(5)\text{--Ni}(2)\text{--N}(7)$		171.6(2)	
$\text{N}(5)\text{--Ni}(2)\text{--N}(8)$		93.9(2)	
$\text{N}(6)\text{--Ni}(2)\text{--N}(7)$		94.3(2)	
$\text{N}(6)\text{--Ni}(2)\text{--N}(8)$		88.8(2)	
$\text{N}(7)\text{--Ni}(2)\text{--N}(8)$		79.6(2)	

el(II) ion is coordinated by one amidate $\text{N}(1)$, one tertiary amine $\text{N}(2)$, and one pyridine $\text{N}(3)$ nitrogen atom as well as a phenolate oxygen atom $\text{O}(1)$. The $\text{Ni}\text{--O}(1)$ bond length is $1.823(1)$ Å; $\text{Ni}(1)\text{--N}(1)$ is 1.822 Å, $\text{Ni}(1)\text{--N}(2)$ is $1.821(1)$ Å, and $\text{Ni}(1)\text{--N}(3)$ is $1.917(1)$ Å. They are much

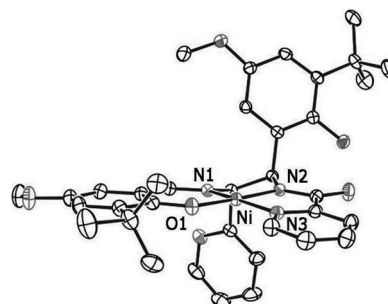


Figure 3. X-ray crystal structure of $[\text{Ni}(\text{L}^6)]$ shown with 30% thermal ellipsoids. H atoms are omitted for clarity.

shorter than those obtained for $[\text{Ni}(\text{L}^2)_2]$ and $[\text{Ni}(\text{L}^5)_2]$, thus showing that the nickel(II) atom is within a different spin configuration, i.e. $S = 0$. The $\text{O}(1)\text{--Ni}(1)\text{--N}(1)$, $\text{O}(1)\text{--Ni}(1)\text{--N}(2)$, $\text{N}(1)\text{--Ni}(1)\text{--N}(2)$, and $\text{N}(2)\text{--Ni}(1)\text{--N}(3)$ angles differ only slightly from 90° , whereas the $\text{O}(1)\text{--Ni}(1)\text{--N}(2)$ and $\text{N}(1)\text{--Ni}(1)\text{--N}(3)$ angles are close to 180° . The geometry around the metal center is thus square-planar, in agreement with a low-spin configuration of the nickel ion. We did not further investigate the properties of $[\text{Ni}(\text{L}^6)]$ because of the low yield of crystallization, as well as the irreversibility of the CV curves obtained from preliminary electrochemical studies.

The coordination modes of $[\text{Ni}(\text{L}^{1-3})_2]$ have also been investigated by calculations using the GAUSSIAN suite at the DFT B3LYP/LANL2DZ level of theory.^[8b,9,11]

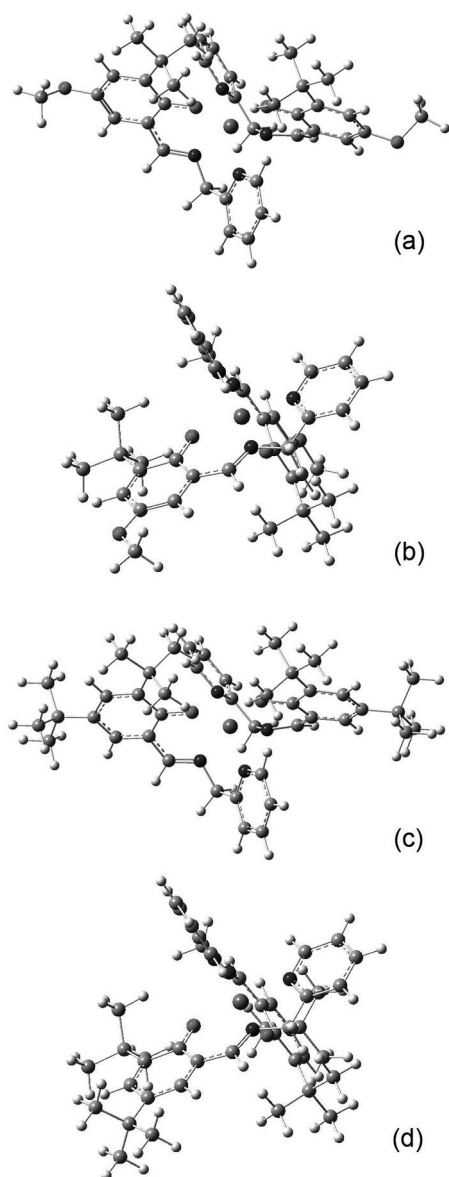


Figure 4. Optimized structures for *fac*- $[\text{Ni}(\text{L}^1)_2]$ (a), *mer*- $[\text{Ni}(\text{L}^1)_2]$ (b), *fac*- $[\text{Ni}(\text{L}^2)_2]$ (c), and *mer*- $[\text{Ni}(\text{L}^2)_2]$ (d).

The meridional versus facial preference in $[\text{Ni}(\text{L}^{1-3})_2]$ was studied by computing differences in energies for the *mer*- and *fac*-isomeric pairs. Optimized geometries for the *mer* and *fac* structures are depicted in Figures 4 and 5. The optimized bond lengths and angles of *mer*- $[\text{Ni}(\text{L}^2)_2]$ were found to be in perfect agreement with the crystal structure. For both $[\text{Ni}(\text{L}^1)_2]$ and $[\text{Ni}(\text{L}^2)_2]$ the *mer* isomer was found to be more stable than the *fac* one as observed experimentally. The energy difference was calculated to be $12.9 \text{ kcal mol}^{-1}$ and $9.7 \text{ kcal mol}^{-1}$ for $[\text{Ni}(\text{L}^1)_2]$ and $[\text{Ni}(\text{L}^2)_2]$, respectively. In contrast, *mer*- $[\text{Ni}(\text{L}^3)_2]$ is found to be $2.0 \text{ kcal mol}^{-1}$ less stable than *cis, fac*- $[\text{Ni}(\text{L}^3)_2]$. The energy reversal of more than 10 kcal mol^{-1} makes the meridional coordination favored in $[\text{Ni}(\text{L}^1)_2]$ and $[\text{Ni}(\text{L}^2)_2]$. This is attributed to the rigidity of the deprotonated ligands L^1 and L^2 .^[9] Similar results have been reported for the iron complex of HL^1 where the *mer* isomer was more stable than the *fac* one by $8.5 \text{ kcal mol}^{-1}$.^[9] We have also investigated the *cis* versus *trans* preference in *fac*- $[\text{Ni}(\text{L}^3)_2]$ (Figure 5). The *trans, fac*- $[\text{Ni}(\text{L}^3)_2]$ isomer was found to be $5.2 \text{ kcal mol}^{-1}$ more stable than the *cis, fac*- $[\text{Ni}(\text{L}^3)_2]$ isomer, which is ascribed to steric hindrances between the *tert*-butyl groups of the phenolate moieties.

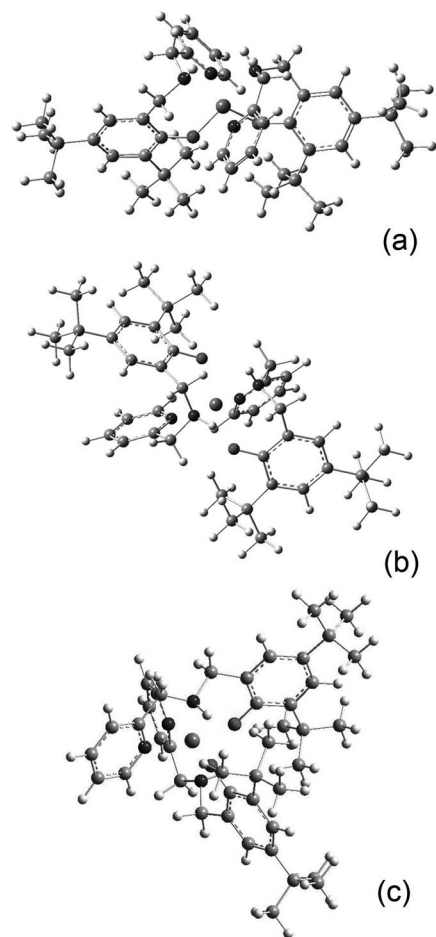


Figure 5. Optimized structures for *cis, fac*- $[\text{Ni}(\text{L}^3)_2]$ (a), *trans, fac*- $[\text{Ni}(\text{L}^3)_2]$ (b), and *mer*- $[\text{Ni}(\text{L}^3)_2]$ (c).

Spectroscopic and Electrochemical Properties of the Nickel Complexes

The five complexes $[\text{Ni}(\text{L}^{1-5})_2]^+$ exhibit ^1H NMR spectroscopic resonances distributed over a wide spectral width ($\delta = 0$ to 50 ppm). They are thus paramagnetic, high-spin Ni^{II} species, confirming that the nickel ion retains its pseudo-octahedral geometry in solution. Despite being paramagnetic, no signal could be observed in their X-band EPR spectra. This paradox is explained by the fact that high-spin nickel(II) complexes usually exhibit zero-field-splitting parameters larger than the X-band quantum (0.3 cm^{-1}). They are consequently not detectable by conventional EPR spectroscopy.^[12]

The electronic spectra of $[\text{Ni}(\text{L}^{1-5})_2]$ are shown in Figure 6. The spectra of $[\text{Ni}(\text{L}^{1-2})_2]$ are characterized by an intense absorption that results from a combination of $\pi\text{-}\pi^*$ and charge-transfer transitions. This absorption is observed at 438 nm ($\epsilon = 14600 \text{ M}^{-1}\text{cm}^{-1}$) for $[\text{Ni}(\text{L}^1)_2]$ and 418 nm ($16000 \text{ M}^{-1}\text{cm}^{-1}$) for $[\text{Ni}(\text{L}^2)_2]$. This shift of λ_{max} reflects the lower electron-donating properties of the *tert*-butyl group relative to the methoxy *para* substituent. In $[\text{Ni}(\text{L}^{4-5})_2]$ the absorption is observed at an even longer wavelength [529 nm ($31000 \text{ M}^{-1}\text{cm}^{-1}$) and 508 nm ($32000 \text{ M}^{-1}\text{cm}^{-1}$), respectively] as a result of an extended conjugation between the quinoline and the phenolate moiety. No such intense absorption could be observed in the visible spectrum of $[\text{Ni}(\text{L}^3)_2]$, highlighting the contribution of the imino-phenolate orbitals to this transition. The nickel(II) d-d transitions could be observed as low intensity bands in the 540–578 nm region for $[\text{Ni}(\text{L}^{1-3})_2]$, while they are hidden by higher intensity transitions involving the ligand orbitals in $[\text{Ni}(\text{L}^{4-5})_2]$.

The electrochemical behavior of $[\text{Ni}(\text{L}^{1-5})_2]$ has been studied in CH_2Cl_2 by cyclic voltammetry (CV). All the potential values are given relative to the Fc^+/Fc reference electrode.

The CV curves of $[\text{Ni}(\text{L}^{1-5})_2]$ exhibit two reversible oxidation waves (Figure 7). Each redox process corresponds to a one-electron transfer, which was confirmed by a coulometric titration and a rotating disc electrode (RDE) amperometric titration (Figures S1–S5). The corresponding potentials are $E_{1/2}^1 = -0.17 \text{ V}$ and $E_{1/2}^2 = 0.08 \text{ V}$ for $[\text{Ni}(\text{L}^1)_2]$ and $E_{1/2}^1 = -0.01 \text{ V}$ and $E_{1/2}^2 = 0.32 \text{ V}$ for $[\text{Ni}(\text{L}^2)_2]$. The higher values obtained for $[\text{Ni}(\text{L}^2)_2]$ result from the lower electron-donating properties of the *tert*-butyl group relative to the methoxy group. A participation of the ligand in the oxidation locus of the complexes is thus expected.

$[\text{Ni}(\text{L}^3)_2]$ exhibits oxidation potentials at $E_{1/2}^1 = -0.20 \text{ V}$ and $E_{1/2}^2 = 0.09 \text{ V}$. These values are much lower than those of $[\text{Ni}(\text{L}^2)_2]$, in agreement with the electron-withdrawing effect of the conjugated imine. Most of all, they are very close to those obtained for $[\text{Ni}(\text{L}^1)_2]$ showing that the replacement of the imine by an aminomethyl group efficiently counterbalances the lower electron-donating properties of the *tert*-butyl versus methoxy substituent.

The CV curves of $[\text{Ni}(\text{L}^4)_2]$ and $[\text{Ni}(\text{L}^5)_2]$ are characterized by two oxidation waves at $E_{1/2}^1 = -0.09 \text{ V}$, $E_{1/2}^2 =$

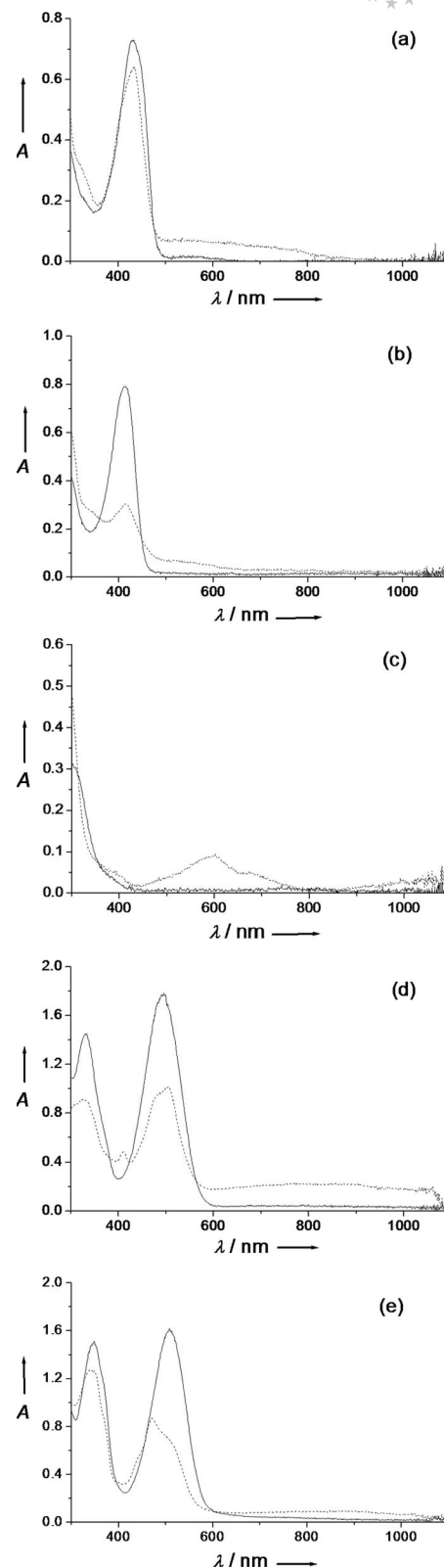


Figure 6. Electronic spectra (233 K) of 0.05 mM CH_2Cl_2 solutions (+ 5 mM TBAP) of: (a) $[\text{Ni}(\text{L}^1)_2]$ (solid line), $[\text{Ni}(\text{L}^1)_2]^+$ (dashed line); (b) $[\text{Ni}(\text{L}^2)_2]$ (solid line), $[\text{Ni}(\text{L}^2)_2]^+$ (dashed line); (c) $[\text{Ni}(\text{L}^3)_2]$ (solid line), $[\text{Ni}(\text{L}^3)_2]^+$ (dashed line); (d) $[\text{Ni}(\text{L}^4)_2]$ (solid line), $[\text{Ni}(\text{L}^4)_2]^+$ (dashed line); (e) $[\text{Ni}(\text{L}^5)_2]$ (dotted line); $[\text{Ni}(\text{L}^5)_2]^+$ (solid line); path length is 1.000 cm; the samples were electrochemically generated in CH_2Cl_2 + 0.1 M TBAP solutions and diluted 20-fold in CH_2Cl_2 .

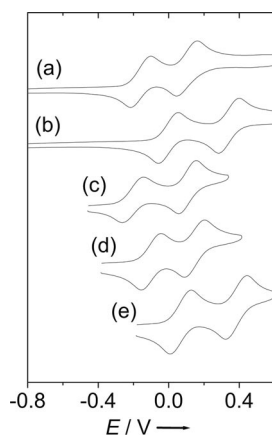


Figure 7. Cyclic voltammograms of 1 mM solutions of the complexes in CH_2Cl_2 containing 0.1 M TBAP. (a) $[\text{Ni}(\text{L}^1)_2]$, (b) $[\text{Ni}(\text{L}^2)_2]$, (c) $[\text{Ni}(\text{L}^3)_2]$, (d) $[\text{Ni}(\text{L}^4)_2]$, (e) $[\text{Ni}(\text{L}^5)_2]$. Scan rate: 0.1 V s^{-1} , $T = 298 \text{ K}$ {except $[\text{Ni}(\text{L}^3)_2]$ recorded at 233 K }. The potentials are referenced vs. the Fc/Fc^+ couple.

0.16 V and $E_{1/2}^1 = 0.08 \text{ V}$, $E_{1/2}^2 = 0.40 \text{ V}$, respectively. They are shifted according to the electronic properties of the phenolate *para* substituent as in $[\text{Ni}(\text{L}^1)_2]$ and $[\text{Ni}(\text{L}^2)_2]$. By comparing the $E_{1/2}$ values obtained for $[\text{Ni}(\text{L}^1)_2]$ and those obtained for $[\text{Ni}(\text{L}^4)_2]$ it appears that the substitution of a pyridine by a quinoline group makes the complexes slightly harder to oxidize. The same observation prevails when the $E_{1/2}$ value obtained for $[\text{Ni}(\text{L}^2)_2]$ is compared with that of $[\text{Ni}(\text{L}^5)_2]$. In contrast, no such shifts are observed when the oxidation potentials of the respective free ligands are compared with one another (Table 2). The metal ion, in addition to the ligand, is thus involved in the oxidation pro-

Table 2. UV/Vis and electrochemical properties^[a,b] of $[\text{Ni}(\text{L}^{1-5})_2]$.

Complex	λ_{max} [nm] (ϵ [$\text{M}^{-1} \text{cm}^{-1}$]) ^[c]	$E_{1/2}^1$	$E_{1/2}^2$
$[\text{Ni}(\text{L}^1)_2]$	438 (14600), 544 (360)	-0.176	0.088
$[\text{Ni}(\text{L}^2)_2]$	418 (16000), 540 sh (150)	-0.028	0.33
$[\text{Ni}(\text{L}^3)_2]$	310 (12910), 578 (26)	-0.204	0.088
$[\text{Ni}(\text{L}^4)_2]$	350 (27000), 529 (31000)	-0.088	0.16
$[\text{Ni}(\text{L}^5)_2]$	350 (30000), 508 (32000)	0.08	0.396

[a] In CH_2Cl_2 (+ 0.1 M TBAP) at 298 K. Potential values in V vs. the Fc^+/Fc reference electrode. The $E_{1/2}$ values were obtained from differential pulse voltammetry (DPV) curves by adding half of the pulse amplitude to the E^p value (pulse amp. 50 mV). The confidence level is $\pm 0.005 \text{ V}$. [b] For the ligands HL^1 , HL^2 , HL^3 , HL^4 , and HL^5 the E^p values obtained from DPV curves are 0.307, 0.511, 0.215, 0.319, and 0.503 V, respectively. [c] In CH_2Cl_2 at 298 K.

Table 3. UV/Vis properties^[a] of complexes $[\text{Ni}(\text{L}^{1-5})_2]^+$.

Complex	λ_{max} [nm] (ϵ [$\text{M}^{-1} \text{cm}^{-1}$])
$[\text{Ni}(\text{L}^1)_2]^+$	316 sh (6560), 433 (12740), 553 br (1380), 660 br (1080)
$[\text{Ni}(\text{L}^2)_2]^+$	347 sh (5320), 398 sh (5420), 414 (6100), 523 br (1380), 588 br (1100)
$[\text{Ni}(\text{L}^3)_2]^+$	390 sh (5400), 595 (8900), 680 sh (4900), >1050 br (>4000)
$[\text{Ni}(\text{L}^4)_2]^+$	328 (18220), 411 (9680), 482 sh (19000), 504 (20360), 800 br (4000)
$[\text{Ni}(\text{L}^5)_2]^+$	341 (25480), 448 sh (11720), 471 (17360), 505 sh (14100), 800 br (1900)

[a] In CH_2Cl_2 (+ 5 mM TBAP) at 233 K. The samples were electrochemically generated in CH_2Cl_2 + 0.1 M TBAP solutions and diluted 20-fold in CH_2Cl_2 .

cess. It is also noticeable that the oxidation potentials are lower than most of those reported for nickel complexes of salen and reduced salen ligands.^[4b,4d-4j]

Spectroscopic Properties of the One-Electron-Oxidized Nickel Complexes

The one-electron-oxidized complexes $[\text{Ni}(\text{L}^{1-5})_2]^+$ have been generated electrochemically in CH_2Cl_2 (+ 0.1 M TBAP) at 233 K.

Upon electrolysis, the brown solutions of $[\text{Ni}(\text{L}^1)_2]$ and $[\text{Ni}(\text{L}^2)_2]$ take on an orange shade. The quantitative generation of the cations (>95%) was evident by RDE amperometric titration: the anodic wave observed at -0.18 and -0.03 V for $[\text{Ni}(\text{L}^1)_2]$ and $[\text{Ni}(\text{L}^2)_2]$, respectively, is progressively replaced by a cathodic wave at the same potential (Figures S1–S5).

The UV/Vis spectrum of $[\text{Ni}(\text{L}^1)_2]^+$ is characterized by an intense absorption band at 433 nm [$12740 \text{ M}^{-1} \text{cm}^{-1}$] and lower intensity broad transitions in the 500–700 nm region (Table 3). The spectrum of $[\text{Ni}(\text{L}^2)_2]^+$ also exhibits an intense absorption band at a somewhat lower wavelength (414 nm [$6100 \text{ M}^{-1} \text{cm}^{-1}$]) and low intensity transitions in the 500–700 nm region (Figure 6, Table 3). The intense π - π^* transitions of a phenoxyl radical, if it is present, are expected to be found in the 390–440 nm region.^[13] As the initial complexes $[\text{Ni}(\text{L}^1)_2]$ and $[\text{Ni}(\text{L}^2)_2]$ already possess a strong absorption band at 431 and 413 nm, respectively, it is not possible to conclude unambiguously to a ligand-based rather than metal-based oxidation process in these cases.

The colorless CH_2Cl_2 solution of $[\text{Ni}(\text{L}^3)_2]$ rapidly turns blue upon one-electron oxidation. $[\text{Ni}(\text{L}^3)_2]^+$ exhibits intense absorption bands at around 390 nm as a shoulder ($5400 \text{ M}^{-1} \text{cm}^{-1}$), 595 nm ($8900 \text{ M}^{-1} \text{cm}^{-1}$), 680 nm (shoulder, $4900 \text{ M}^{-1} \text{cm}^{-1}$), and >1050 nm ($>4000 \text{ M}^{-1} \text{cm}^{-1}$) (Table 3). These transitions resemble those reported for phenoxyl radical species obtained by electrochemical oxidation of either the *N,N'*-bis{2,4-di-*tert*-butyl-phenol}ethylenediamine ligand or its copper(II) complex, and 2-imidazole-4,6-di-*tert*-butylphenoxyl radicals.^[14] These bands could thus be safely attributed to the π - π^* transitions of a coordinating phenoxyl radical.

The visible spectrum of $[\text{Ni}(\text{L}^4)_2]^+$ is characterized by intense absorption bands at 411 nm ($9680 \text{ M}^{-1} \text{cm}^{-1}$) and 504 nm ($20360 \text{ M}^{-1} \text{cm}^{-1}$), with a low-intensity broad transition at 800 nm ($4000 \text{ M}^{-1} \text{cm}^{-1}$). The spectrum of $[\text{Ni}(\text{L}^5)_2]^+$

exhibits absorption bands at 448 nm ($11720 \text{ M}^{-1} \text{ cm}^{-1}$), 471 nm ($17360 \text{ M}^{-1} \text{ cm}^{-1}$), and 800 nm ($1900 \text{ M}^{-1} \text{ cm}^{-1}$) (Table 3). The well-resolved 411 nm absorption in the visible spectrum of $[\text{Ni}(\text{L}^4)_2]^+$, which is absent in the spectrum of $[\text{Ni}(\text{L}^4)_2]$, is typical for copper(II)- or nickel(II)-coordinated phenoxyl radicals.

EPR spectroscopy has been used to probe more finely the oxidation sites in $[\text{Ni}(\text{L}^{1-5})_2]^+$ and confirm the trends deduced from UV/Vis spectroscopy.

The EPR spectrum of $[\text{Ni}(\text{L}^1)_2]^+$ in frozen CH_2Cl_2 exhibits a dominant $S = 1/2$ signal at $g = 2.21$ (Figure 8a). It is found to be nearly isotropic and identical to that reported by Shimazaki et al. for an $S = 1/2$ complex involving a high-spin nickel(II) complex coordinated to a phenoxyl radical.^[4c] This signal is thus taken as evidence for an antiferromagnetic coupling between a high-spin Ni^{II} ion and a phenoxyl radical leading to an $S = 1/2$ system. Such a high g_{average} value for an $S = 1/2$ system has also been reported recently for a complex involving a high-spin nickel(II) antiferromagnetically coupled to a copper(II) center^[15] or an iminosemiquinone radical moiety.^[3i]

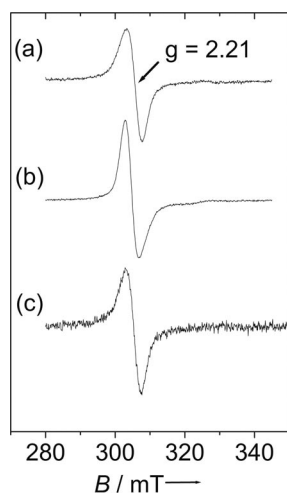


Figure 8. X-band EPR spectra of 1 mM CH_2Cl_2 (+ 0.1 M TBAP) solutions of: (a) $[\text{Ni}(\text{L}^1)_2]^+$, (b) $[\text{Ni}(\text{L}^3)_2]^+$, (c) $[\text{Ni}(\text{L}^4)_2]^+$. $T = 100 \text{ K}$, microwave frequency 9.42 GHz, power 20 mW, modulation frequency 100 kHz, amplitude 0.197 mT.

The EPR spectrum of $[\text{Ni}(\text{L}^2)_2]^+$ contrasts sharply with that of $[\text{Ni}(\text{L}^1)_2]^+$: The $S = 1/2$ signal was found to be clearly anisotropic with g values of $g_1 = 2.205$, $g_2 = 2.113$, and $g_3 = 2.053$ ($g_{\text{av}} = 2.12$, Figure 9a). In addition, a hyperfine coupling resulting from the interaction of the electron with two equivalent nitrogen atoms could be resolved in the g_3 component ($A_3^{(2\text{N})} = 2.0 \text{ mT}$). This suggests that the contribution of the metal orbital to the SOMO is much more significant in $[\text{Ni}(\text{L}^2)_2]^+$ than in $[\text{Ni}(\text{L}^1)_2]^+$. The ordering of g is also consistent with a ground state that is essentially $d_{x^2-y^2}$.^[7i] This ground state is remarkable as most of the pseudo-octahedral Ni^{III} complexes of tetradentate Schiff base ligands with two axially bound exogenous pyridine rings (thus involving the same donor set, two N_{py} , two N_{im} and two O_{phO} atoms) exhibit a d_{z^2} ground state

(axially elongated rather than axially compressed, Figure 9c).^[4b,4c-4j,7] The ground state could thus be efficiently modulated by controlling pyridine ligation. The observed inversion in $[\text{Ni}(\text{L}^2)_2]^+$ may result from the higher axial ligand field provided by the rigid tridentate ligands.

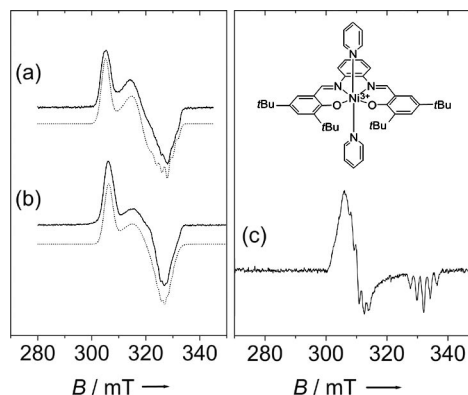


Figure 9. X-band EPR spectra of 1 mM solution in CH_2Cl_2 containing 0.1 M TBAP of: (a) $[\text{Ni}(\text{L}^2)_2]^+$ (solid lines) and simulation using parameters given in the text (dotted lines); (b) $[\text{Ni}(\text{L}^5)_2]^+$ (solid lines) and simulation using parameters given in the text (dotted lines); (c) the pseudo-octahedral Ni^{III} complex of a tetradentate Schiff base ligand with two axially bound exogenous pyridine rings.^[4f] The chemical formula is shown at the top. $T = 100 \text{ K}$, microwave frequency 9.42 GHz, power 20 mW, modulation frequency 100 kHz, amplitude 0.197 mT.

$[\text{Ni}(\text{L}^3)_2]^+$ exhibits an EPR signal close to that observed for $[\text{Ni}(\text{L}^1)_2]^+$ (Figure 8b) although it is slightly more anisotropic.^[16] An electronic structure similar to that of $[\text{Ni}(\text{L}^1)_2]^+$ thus prevails, despite the fact that the ligands differ both by their phenolate *para* substituent and the pivotal nitrogen atom.

It is important to remark that the EPR signatures of the $[\text{Ni}(\text{L}^{1-3})_2]^+$ cations are correlated with the oxidation potential of the starting neutral compounds: The lower oxidation potentials are indicative of an oxidation process that is ligand-centered, while the higher oxidation potentials are indicative of a metal-centered oxidation process.

The EPR spectra of $[\text{Ni}(\text{L}^4)_2]^+$ and $[\text{Ni}(\text{L}^5)_2]^+$ in frozen CH_2Cl_2 compare with those of $[\text{Ni}(\text{L}^1)_2]^+$ and $[\text{Ni}(\text{L}^2)_2]^+$, respectively, (Figures 8c and 9b). The global electronic distribution is thus poorly affected by changes in the N-donor properties of the pyridine group. The parameters obtained by simulation of the spectrum of $[\text{Ni}(\text{L}^2)_2]^+$ differ somewhat slightly from those obtained for $[\text{Ni}(\text{L}^5)_2]^+$: The g values are $g_1 = 2.195$, $g_2 = 2.103$, and $g_3 = 2.058$ (Figure 9b). As for $[\text{Ni}(\text{L}^2)_2]^+$, a hyperfine coupling resulting from the interaction of the electron with two equivalent nitrogen atoms could be resolved in the g_3 component ($A_3^{(2\text{N})} = 1.4 \text{ mT}$). This behavior is in agreement with changes in the donor properties of a coordinating nitrogen atom and indicates that at least one nitrogen atom of the ligand remains coordinated to the metal ion after one-electron oxidation.

EPR spectra have also been recorded in a $\text{CH}_2\text{Cl}_2/\text{CH}_3\text{OH}$ mixture, i.e. in the presence of a moderately coordinating solvent.^[17]

The spectra were found to be similar to those obtained in neat CH_2Cl_2 (Figure S6). This is an important result as most of the one-electron-oxidized nickel–salen complexes are extremely sensitive to traces of coordinating solvents. In particular, CH_3OH , which is known to bind tightly to the nickel ion, promotes an intramolecular electron transfer from the metal atom to the Schiff base ligand.^[4b,4e–4i,7] Consequently, nickel(II)–phenoxyl radical complexes of tetradentate Schiff bases are always converted into nickel(III) species in the presence of CH_3OH . The metal ion in $[\text{Ni}(\text{L}^{1-5})_2]^+$ is already hexacoordinate. Binding of additional low-affinity exogenous ligands is no longer possible, thus preventing subsequent solvent-dependent valence tautomerism.

Changes in the phenolate *para* substituent or in the hybridization of the pivotal nitrogen atom thus dramatically influence the EPR spectra of the cations. In contrast changes in the N-donor properties of the imino terminal nitrogen atom (quinoline to pyridine substitution) do not significantly affect the EPR signature of the cations.

Conclusions

We have described the oxidation behavior of five nickel(II) complexes of tridentate Schiff base ligands $[\text{Ni}(\text{L}^{1-5})_2]$. In this series, the ligands differ from one another by the phenolate *para* substituent, the hybridization of the pivotal nitrogen atom, and the N-donor properties of the terminal pyridine group.

$[\text{Ni}(\text{L}^1)_2]$ is characterized by an oxidation potential at -0.17 V vs. Fc^+/Fc . The one-electron-oxidized species $[\text{Ni}(\text{L}^1)_2]^+$ exhibits an EPR signal at $g = 2.21$ similar to that reported for Ni^{II} –radical complexes of tripodal ligands (high-spin Ni^{II} antiferromagnetically coupled to a phenoxyl radical).^[4c] $[\text{Ni}(\text{L}^2)_2]$ differs from $[\text{Ni}(\text{L}^1)_2]$ by the phenolate *para* substituent (*tert*-butyl instead of methoxy group) and exhibits an oxidation potential that is ca. 0.16 V higher. The electrogenerated cation $[\text{Ni}(\text{L}^2)_2]^+$ is characterized by a significant contribution of a metal orbital to the SOMO and an unusual $d_{x^2-y^2}$ ground state. The oxidation site is thus shifted from the ligand to the metal atom by lowering the electron-donating properties of the phenolate *para* substituent. $[\text{Ni}(\text{L}^3)_2]^+$ exhibits both an EPR and an electrochemical signature similar to those of $[\text{Ni}(\text{L}^1)_2]^+$ indicating that the imino to amino substitution compensates exactly for the methoxy to *tert*-butyl one.

The influence of the pendant pyridine ring in $[\text{Ni}(\text{L}^{1-2})_2]$ has been studied by replacing it by a quinoline group $\{[\text{Ni}(\text{L}^{4-5})_2]$ compounds $\}$. This change does not significantly affect the EPR signature of the cations, but makes the complexes slightly harder to oxidize.

Finally, there are fundamental differences in the oxidation behavior of the nickel complexes according to whether they are synthesized from one tetradentate (low-spin configuration of the metal ion) or two tridentate (high-spin configuration of the metal ion) Schiff base ligands:

One-electron oxidation of square-planar nickel complexes of tetradentate Schiff bases affords radical species

with partial delocalization of the SOMO onto the metal orbitals. A *tert*-butyl to $\text{N}(\text{CH}_3)_2$ substitution^[18] at the *para* position of the phenolate induces a small but detectable shift of the SOMO.^[4j] The contribution of the metal atom decreases from 6.6 to 1.8%. This substitution also results in a very large drop of the oxidation potential (from 0.582 to -0.144 V vs. Fc^+/Fc). In the $[\text{Ni}(\text{L}^{1-5})_2]$ series a *tert*-butyl to methoxy substitution is sufficient^[17] to dramatically shift the oxidation site from the metal atom to the ligand, i.e. to promote a “chemical valence tautomerism”.^[3e] In addition this phenomenon is observed within a narrower range of potentials {the oxidation potentials are -0.028 and -0.176 V for $[\text{Ni}(\text{L}^1)_2]$ and $[\text{Ni}(\text{L}^2)_2]$, respectively}.

Pyridine or any exogenous ligand could be added to the nickel complexes of tetradentate Schiff bases in order to obtain a pseudo-octahedral metal ion. Unfortunately, this geometrical change is irremediably accompanied by a valence tautomerism making the oxidation locus strongly solvent-dependent: Axial coordination shifts the d_{z^2} orbital to a higher energy, resulting in the transfer of an electron from the metal center to the ligand. The oxidation state of the nickel ion in the so-obtained pseudo-octahedral complex is +III, and the ground state is d_{z^2} [nickel(III) complexes that exhibit a $d_{x^2-y^2}$ ground state exist but they are rare]. In contrast, $[\text{Ni}(\text{L}^{1-5})_2]^+$ exhibit an oxidation locus that is fully insensitive to the solvent. This is the result of an environment of the metal atom in $[\text{Ni}(\text{L}^{1-5})_2]^+$ that is already pseudo-octahedral, and the fact that solvent molecules are not able to displace one of the tridentate ligands (chelate effect). It is thus possible to cancel the “solvent-dependent valence tautomerism” simply by changing the denticity of the Schiff bases in the nickel complexes. Moreover, $[\text{Ni}(\text{L}^2)_2]^+$ and $[\text{Ni}(\text{L}^5)_2]^+$ exhibit a $d_{x^2-y^2}$ ground state, which is rather unusual. It may result from the higher axial ligand field provided by two tridentate ligands compared to one tetradentate ligand plus two pyridine groups.

The oxidative chemistry of apparently simple Schiff base nickel complexes is thus full of surprises. Complexes from tridentate Schiff bases exhibit an unprecedented oxidative behavior that contrasts sharply with that of more common tetradentate ones. A simple change in the denticity of the ligand thus has strong consequences on the oxidation behavior of the nickel complexes. Actually, it is uncertain whether the $[\text{Ni}(\text{L}^{1-5})_2]^+$ series constitutes the exception that proves the rule or if it reflects a more general trend.

Further studies concerning the rearrangement mechanism of $[\text{Ni}(\text{L}^1)_2]$ into $[\text{Ni}(\text{L}^6)]$, and the effect of the ligand/metal stoichiometry on the nickel spin state are currently in progress.

Experimental Section

Materials and Methods: All chemicals were of reagent grade and were used without purification. CH_2Cl_2 was anhydrous ($>99.8\%$) and stored under argon. NMR spectra were recorded with a Bruker AM 300 (^1H NMR at 300 MHz) spectrometer. Chemical shifts are quoted relative to tetramethylsilane (TMS). Mass spectra were recorded with a Thermofininger (EI/DCI) or a Nermag R101C

(FAB+) apparatus. Low-temperature UV/Vis spectra were recorded with a Cary Varian 50 spectrophotometer equipped with a low-temperature Hellma immersion probe (1.000 cm path length). The temperature was set at 238 K with an RK8 KS Lauda cryostat. X-band EPR spectra were recorded with a Bruker ESP 300E spectrometer equipped with a Bruker nitrogen flow cryostat. Spectra were treated by using the WINEPR software and simulated by using the Bruker SIMFONIA software. Electrochemical measurements were carried out by using a CHI110 potentiostat. Experiments were performed in a standard three-electrode cell under argon. An Ag/AgNO₃ (0.01 M) reference electrode was used. All the potentials given in the text refer to the regular Fc/Fc⁺ redox couple used as an internal reference. A glassy carbon disc electrode (5 mm diameter), which was polished with 1 mm diamond paste, was used as the working electrode. The electrochemical behavior of the ligands and complexes was studied by cyclic voltammetry (CV) and with a rotating disc electrode (RDE) in CH₂Cl₂ solutions containing 0.1 M tetrabutylammonium perchlorate (TBAP) as the supporting electrolyte. Electrolysis was performed at 233 K by using a PAR model 273 potentiostat and a carbon felt working electrode.

Crystal Structure Analysis: Crystals were mounted on a Kappa CCD Nonius diffractometer equipped with graphite-monochromated Mo-*K*_α radiation ($\lambda = 0.71073 \text{ \AA}$) and a cryostream cooler. The collected reflections were corrected for Lorentzian and polarization effects but not for absorption. Crystal structural solution (direct method) and refinement (by full-matrix least squares on *F*) was performed by using the *teXsan* analysis package. All non-hydrogen atoms were refined with anisotropic thermal parameters. Hydrogen atoms were generated in idealized positions, riding on the carrier atoms, with isotropic thermal parameters. CCDC-642613, -659639, and -659640 contain the supplementary crystallographic data for this paper. These data can be obtained free of charge from the Cambridge Crystallographic Data Center via www.ccdc.cam.ac.uk/datarequest/cif.

Crystal Data

[Ni(L²)₂]: Red prism (0.3 × 0.2 × 0.1 mm), *M_r* = 705.61 g mol⁻¹, monoclinic, space group *P*2₁/*c*, *a* = 10.291(1) Å, *b* = 22.160(4) Å, *c* = 17.723(5) Å, $\alpha = 90^\circ$, $\beta = 96.2(3)^\circ$, $\gamma = 90^\circ$, *V* = 3956(1) Å³, *Z* = 4, *D_c* = 1.185 g cm⁻³, *T* = 293 K, $\mu(\text{Mo-}K_\alpha) = 5.29 \text{ cm}^{-1}$. 59876 reflections were collected. Of the 11799 unique reflections (*R*_{int} = 0.16571), 6852 were observed [*F* ≥ 2σ(*F*)] and used in the full-matrix least-squares refinement of 442 variables. *R* = 0.0542, *R_w* = 0.0805, goodness of fit *S* = 0.746, max./min. residual peaks are 1.14/−0.61 e Å⁻³.

[Ni(L⁵)₂]: Red platelet (0.4 × 0.3 × 0.02 mm), *M_r* = 1555.36 g mol⁻¹, triclinic, space group *P*1̄, *a* = 15.514(4) Å, *b* = 15.742(2) Å, *c* = 17.882(5) Å, $\alpha = 90.15(2)^\circ$, $\beta = 102.48(2)^\circ$, $\gamma = 101.37(2)^\circ$, *V* = 4176(2) Å³, *Z* = 2, *D_c* = 1.237 g cm⁻³, *T* = 150 K, $\mu(\text{Mo-}K_\alpha) = 5.08 \text{ cm}^{-1}$. 59876 reflections were collected. Of the 71767 unique reflections (*R*_{int} = 0.21943), 7407 were observed [*F* ≥ 2σ(*F*)] and used in the full-matrix least-squares refinement of 991 variables. *R* = 0.0703, *R_w* = 0.0740, goodness of fit *S* = 1.250, max./min. residual peaks are 0.83/−0.72 e Å⁻³.

[Ni(L⁶)]: Red prism (0.4 × 0.3 × 0.1 mm), *M_r* = 699.48 g mol⁻¹, triclinic, space group *P*1, *a* = 9.2525(9) Å, *b* = 14.2426(4) Å, *c* = 15.476(1) Å, $\alpha = 116.572(4)^\circ$, $\beta = 105.421(8)^\circ$, $\gamma = 78.773(5)^\circ$, *V* = 1751.5(2) Å³, *Z* = 2, *D_c* = 1.326 g cm⁻³, *T* = 293 K, $\mu(\text{Mo-}K_\alpha) = 6.05 \text{ cm}^{-1}$. Of the 10101 unique reflections (*R*_{int} = 0.06128), 7324 were observed [*F* ≥ 2σ(*F*)] and used in the full-matrix least-squares refinement of 433 variables. *R* = 0.0434, *R_w* = 0.0599, goodness of fit *S* = 1.217, max./min. residual peaks are 0.65/−0.48 e Å⁻³.

Preparation of the Ligands and Complexes

HL¹: 2-Picolylamine (340 mg, 3.16 mmol) was added to a stirred solution of 3-*tert*-butyl-2-hydroxy-5-methoxybenzaldehyde (658 mg, 3.16 mmol) in methanol (20 mL). The solution was heated at reflux for 5 h. Removal of the solvent in vacuo yielded a dark-red oil. Addition of pentane (1 mL) afforded a brown solid 15 h later. Yield 820 mg (87%). C₁₈H₂₂N₂O₂ (298.38): calcd. C 72.46, H 7.43, N 9.39; found C 72.35, H 7.41, N 9.58. ¹H NMR (CDCl₃): $\delta = 8.57$ (d, 1 H, ³*J* = 4 Hz), 8.51 (s, 1 H), 7.39 (m, 1 H), 7.21 (m, 2 H), 6.99 (d, 1 H, ⁴*J* = 3.0 Hz), 6.64 (d, 1 H, ⁴*J* = 3.4 Hz), 4.94 (s, 2 H), 3.78 (s, 3 H), 1.42 (s, 9 H) ppm.

HL⁴: 8-Aminoquinoline (278 mg, 1.92 mmol) in methanol (10 mL) was added to a stirred solution of 3-*tert*-butyl-2-hydroxy-5-methoxybenzaldehyde (400 mg, 1.92 mmol) in methanol (15 mL). Two drops of formic acid were added, and the solution was heated to reflux for 4 h. Removal of the solvent in vacuo yielded a dark-red oil. The crude product was purified by alumina column chromatography with hexane/ethyl acetate (8:1). Yield 300 mg (46%). C₂₁H₂₂N₂O₂ (334.41): calcd. C 75.42, H 6.63, N 8.83; found C 75.38, H 6.59, N 8.96. ¹H NMR (CDCl₃): $\delta = 8.98$ (d, 1 H, ³*J* = 2.7 Hz), 8.88 (s, 1 H), 8.17 (d, 1 H, ³*J* = 8.31 Hz), 7.69 (d, 1 H, ³*J* = 8.19 Hz), 7.55 (m, 1 H), 7.46 (m, 2 H), 7.07 (d, 1 H, ⁴*J* = 2.9 Hz), 6.77 (d, 1 H, ⁴*J* = 3.1 Hz), 3.81 (s, 3 H), 1.49 (s, 9 H) ppm.

[Ni(L¹)₂]: A methanolic solution (20 mL) of Ni(OAc)₂·4H₂O (43 mg, 0.15 mmol) and 2 equiv. of triethylamine (90 μL, 0.62 mmol) were added to a stirred solution of HL¹ (92 mg, 0.31 mmol) in methanol (20 mL). The solution was refluxed for 3 h. After removal of half of the solvent, the solution was stored at −20 °C overnight to afford a powder. Washings with cold methanol led to [Ni(L¹)₂]. Yield 41 mg (42%). C₃₆H₄₂N₄O₄Ni (653.44): calcd. C 66.17, H 6.48, N 8.57, Ni 8.98; found C 65.92, H 6.43, N 8.75, Ni 9.02. MS: *m/z* = 653 [M + H]⁺.

[Ni(L²)₂]: This complex was prepared in a similar manner in 40% yield. X-ray quality crystals were obtained by slow evaporation of the solvent from a concentrated solution of [Ni(L²)₂] in MeOH. C₄₂H₅₄N₄O₂Ni (705.60): calcd. C 71.49, H 7.71, N 7.94, Ni 8.32; found C 71.70, H 7.62, N 8.03, Ni 8.10. MS: *m/z* = 705 [M + H]⁺.

[Ni(L³)₂]: This complex was prepared in a similar manner in 55% yield. C₄₂H₅₈N₄O₂Ni (709.63): calcd. C 71.09, H 8.24, N 7.90, Ni 8.27; found C 71.22, H 8.29, N 8.02, Ni 8.12. MS: *m/z* = 709 [M + H]⁺.

[Ni(L⁴)₂]: This complex was prepared in a similar manner in 44% yield. C₄₂H₅₈N₄O₂Ni (725.50): calcd. C 69.53, H 5.84, N 7.72, Ni 8.09; found C 69.82, H 5.69, N 7.96, Ni 8.13. MS: *m/z* = 731 [M + H]⁺.

[Ni(L⁵)₂]: This complex was prepared in a similar manner in 39% yield. C₄₂H₅₈N₄O₂Ni (777.66): calcd. C 74.13, H 7.00, N 7.20, Ni 7.55; found C 74.22, H 7.01, N 7.11, Ni 7.61. MS: *m/z* = 777 [M + H]⁺.

Supporting Information (see footnote on the first page of this article): Voltammetric curves at RDE and differential pulse voltammetries of [Ni(L¹⁻⁵)₂], and EPR spectra of [Ni(L¹⁻⁵)₂]⁺ in CH₂Cl₂/CH₃OH (1:1) solutions.

- [1] a) M. M. Whittaker, J. W. Whittaker, *J. Biol. Chem.* **1988**, 263, 6074; b) N. Ito, S. E. V. Phillips, C. Stevens, Z. B. Ogel, M. J. McPherson, J. N. Keen, K. D. S. Yadav, P. F. Knowles, *Nature* **1991**, 350, 87; c) C. D. Borman, C. G. Saysell, A. Sokolowski, M. B. Twitchett, C. Wright, A. G. Sykes, *Coord. Chem. Rev.* **1999**, 190–192, 771; d) M. J. McPherson, M. R. Parsons, R. K.

- Spooner, C. M. Wilmot, *Handbook of metalloproteins*, John Wiley and Sons, Chichester, **2001**, p. 1272; e) J. W. Whittaker, *Chem. Rev.* **2003**, *103*, 2347.
- [2] a) B. A. Jazdzewski, W. B. Tolman, *Coord. Chem. Rev.* **2000**, *200–202*, 633; b) S. Itoh, M. Taki, S. Fukuzumi, *Coord. Chem. Rev.* **2000**, *198*, 3; c) P. Chaudhuri, K. Wieghardt, *Prog. Inorg. Chem.* **2001**, *50*, 151; d) W. Kaim, *Dalton Trans.* **2003**, 761; e) P. Chaudhuri, K. Wieghardt, T. Weyhermüller, T. K. Paine, S. Mukherjee, C. Mukherjee, *Biol. Chem.* **2005**, *386*, 1023; f) K. Ray, T. Petrenko, K. Wieghardt, F. Neese, *Dalton Trans.* **2007**, 1552; g) F. Thomas, *Eur. J. Inorg. Chem.* **2007**, 2379.
- [3] a) A. Bencini, C. Carbonera, A. Die, M. G. F. Vaz, *Dalton Trans.* **2003**, 1701; b) C. H. Hsieh, I. J. Hsu, C. M. Lee, S. C. Ke, T. Y. Wang, G. H. Lee, Y. Wang, J. M. Chen, J. F. Lee, W. F. Liaw, *Inorg. Chem.* **2003**, *42*, 3925; c) D. Herebian, K. Wieghardt, F. Neese, *J. Am. Chem. Soc.* **2003**, *125*, 10997; d) X. Ottenwaelder, R. Ruiz-Garcia, G. Blondin, R. Carasco, J. Cano, D. Lexa, Y. Journaux, A. Aukauloo, *Chem. Commun.* **2004**, 504; e) H. Ohtsu, K. Tanaka, *Angew. Chem. Int. Ed.* **2004**, *43*, 6301; f) K. S. Min, T. Weyhermüller, E. Bothe, K. Wieghardt, *Inorg. Chem.* **2004**, *43*, 2922; g) H. Ohtsu, K. Tanaka, *Chem. Eur. J.* **2005**, *11*, 3420; h) K. Ray, T. Weyhermüller, F. Neese, K. Wieghardt, *Inorg. Chem.* **2005**, *44*, 5345; i) K. Chlopek, E. Bothe, F. Neese, T. Weyhermüller, K. Wieghardt, *Inorg. Chem.* **2006**, *45*, 6298.
- [4] a) J. Müller, A. Kikuchi, E. Bill, T. Weyhermüller, P. Hildebrandt, L. Ould-Moussa, K. Wieghardt, *Inorg. Chim. Acta* **2000**, *297*, 265; b) Y. Shimazaki, F. Tani, K. Fukui, Y. Naruta, O. Yamauchi, *J. Am. Chem. Soc.* **2003**, *125*, 10513; c) Y. Shimazaki, S. Huth, S. Karasawa, S. Hirota, Y. Naruta, O. Yamauchi, *Inorg. Chem.* **2004**, *43*, 7816; d) T. Glaser, M. Heidemeier, R. Fröhlich, P. Hildebrandt, E. Bothe, E. Bill, *Inorg. Chem.* **2005**, *44*, 5467; e) O. Rotthaus, O. Jarjayes, F. Thomas, C. Philouze, C. Perez Del Vallee, E. Saint-Aman, J. L. Pierre, *Chem. Eur. J.* **2006**, *12*, 2293; f) O. Rotthaus, F. Thomas, O. Jarjayes, C. Philouze, E. Saint-Aman, J. L. Pierre, *Chem. Eur. J.* **2006**, *12*, 6953; g) Y. Shimazaki, T. Yajima, F. Tani, S. Karasawa, K. Fukui, Y. Naruta, O. Yamauchi, *J. Am. Chem. Soc.* **2007**, *129*, 2559; h) L. Benisvy, R. Kannapan, Y. F. Song, S. Milikisyants, M. Huber, I. Mutikainen, U. Turpeinen, P. Gamez, L. Bernasconi, E. J. Baerends, F. Hartl, J. Reedijk, *Eur. J. Inorg. Chem.* **2007**, 637; i) T. Storr, E. C. Wasinger, R. C. Pratt, T. D. P. Stack, *Angew. Chem.* **2007**, *119*, 5290; *Angew. Chem. Int. Ed.* **2007**, *46*, 5198; j) O. Rotthaus, O. Jarjayes, C. Perez Del Valle, C. Philouze, F. Thomas, *Chem. Commun.* **2007**, 4462.
- [5] D. Parker, E. S. Davies, C. Wilson, J. McMaster, *Inorg. Chim. Acta* **2007**, *360*, 203.
- [6] a) O. Kahn, J. P. Launay, *Chemtronics* **1988**, *3*, 140; b) O. Kahn, C. Martinez, *Science* **1998**, *279*, 44; c) P. Gütligh, Y. Garcia, T. Woike, *Coord. Chem. Rev.* **2001**, *219–221*, 839.
- [7] a) K. Goldsby, *J. Coord. Chem.* **1988**, *19*, 83; b) B. de Castro, C. Freire, *Inorg. Chem.* **1990**, *29*, 5113; c) M. A. A. F. de C. T. Carrondo, B. De Castro, A. M. Coelho, D. Domingues, C. Freire, J. Morais, *Inorg. Chim. Acta* **1993**, *205*, 157; d) F. Azevedo, M. A. Carrondo, B. Castro, M. Convery, D. Domingues, C. Freire, M. T. Duarte, K. Nielsen, I. C. Santos, *Inorg. Chim. Acta* **1994**, *219*, 43; e) M. Vilas-Boas, C. Freire, B. de Castro, A. R. Hillman, P. A. Christensen, *Inorg. Chem.* **1997**, *36*, 4929; f) C. Freire, B. de Castro, *Polyhedron* **1998**, *17*, 4227; g) C. Freire, B. de Castro, *J. Chem. Soc., Dalton Trans.* **1998**, 1491; h) I. C. Santos, M. Vilas-Boas, M. F. M. Piedade, C. Freire, M. T. Duarte, B. de Castro, *Polyhedron* **2000**, *19*, 655; i) D. Pinho, P. Gomes, C. Freire, B. de Castro, *Eur. J. Inorg. Chem.* **2001**, 1483; j) Z. Xiao, B. O. Patrick, D. Dolphin, *Inorg. Chem.* **2003**, *42*, 8125.
- [8] a) Y. L. Wong, Y. Yan, E. S. H. Chan, Q. Yang, T. C. W. Mak, D. K. P. Ng, *J. Chem. Soc., Dalton Trans.* **1998**, 3057; b) R. Shakya, C. Imbert, H. P. Hratchian, M. Lanznaster, M. J. Heeg, B. R. McGarvey, M. Allard, H. B. Schlegel, C. N. Verani, *Dalton Trans.* **2006**, 2517.
- [9] C. Imbert, H. P. Hratchian, M. Lanznaster, M. J. Heeg, L. M. Hryhorczuk, B. R. McGarvey, H. B. Schlegel, C. N. Verani, *Inorg. Chem.* **2005**, *44*, 7414.
- [10] P. A. Cameron, V. C. Gibson, C. Redshaw, J. A. Segal, A. J. P. White, D. J. Williams, *J. Chem. Soc., Dalton Trans.* **2002**, 415.
- [11] M. J. Frisch, G. W. Trucks, H. B. Schlegel, G. E. Scuseria, M. A. Robb, J. R. Cheeseman, J. A. Montgomery Jr, T. Vreven, K. N. Kudin, J. C. Burant, J. M. Millam, S. S. Iyengar, J. Tomasi, V. Barone, B. Mennucci, M. Cossi, G. Scalmani, N. Rega, G. A. Petersson, H. Nakatsuji, M. Hada, M. Ehara, K. Toyota, R. Fukuda, J. Hasegawa, M. Ishida, T. Nakajima, Y. Honda, O. Kitao, H. Nakai, M. Klene, X. Li, J. E. Knox, H. P. Hratchian, J. B. Cross, C. Adamo, J. Jaramillo, R. Gomperts, R. E. Stratmann, O. Yazyev, A. J. Austin, R. Cammi, C. Pomelli, J. W. Ochterski, P. Y. Ayala, K. Morokuma, G. A. Voth, P. Salvador, J. J. Dannenberg, V. G. Zakrzewski, S. Dapprich, A. D. Daniels, M. C. Strain, O. Farkas, D. K. Malick, A. D. Rabuck, K. Raghavachari, J. B. Foresman, J. V. Ortiz, Q. Cui, A. G. Baboul, S. Clifford, J. Cioslowski, B. B. Stefanov, G. Liu, A. Liashenko, P. Piskorz, I. Komaromi, R. L. Martin, D. J. Fox, T. Keith, M. A. Al-Laham, C. Y. Peng, A. Nanayakkara, M. Challacombe, P. M. W. Gill, B. Johnson, W. Chen, M. W. Wong, C. Gonzalez, J. A. Pople, *Gaussian 03, Revision C.02*, Gaussian, Inc., Wallingford CT, **2004**.
- [12] a) D. Collison, M. Helliwell, V. M. Jones, F. E. Mabbs, A. J. L. McInnes, P. C. Riedi, G. M. Smith, R. G. Pritchard, W. I. Cross, *J. Chem. Soc. Faraday Trans.* **1998**, *94*, 3019; b) J. Krzystek, J. H. Park, M. W. Meisel, M. A. Hitchman, H. Strateimer, L. C. Brunel, J. Telser, *Inorg. Chem.* **2002**, *41*, 4478; c) G. Rogez, J. N. Rebilly, A. L. Barra, L. Sorace, G. Blondin, N. Kirchner, M. Duran, J. van Slageren, S. Parsons, L. Ricard, A. Marvilliers, T. Mallah, *Angew. Chem.* **2005**, *117*, 1910; *Angew. Chem. Int. Ed.* **2005**, *44*, 1876.
- [13] a) R. Liu, K. Morokuma, A. M. Mebel, M. C. Lin, *J. Phys. Chem.* **1996**, *100*, 9314; b) H. M. Chang, H. H. Jaffe, *Chem. Phys. Lett.* **1973**, *23*, 146; c) H. M. Chang, H. H. Jaffe, C. A. Masmandis, *J. Phys. Chem.* **1975**, *79*, 1118; d) L. J. Johnston, N. Mathivanan, F. Negri, W. Siebrand, F. Zerbetto, *Can. J. Chem.* **1993**, *71*, 1655; e) J. Takahashi, T. Shida, *Bull. Chem. Soc. Jpn.* **1994**, *67*, 2038; f) J. Takahashi, T. Momose, T. Shida, *Bull. Chem. Soc. Jpn.* **1994**, *67*, 964; g) J. G. Radziszewski, M. Gil, A. Gorski, J. Spanget-Larsen, J. Waluk, B. J. Mroz, *J. Chem. Phys.* **2001**, *115*, 9733.
- [14] a) F. Thomas, O. Jarjayes, C. Duboc, C. Philouze, E. Saint-Aman, J. L. Pierre, *Dalton Trans.* **2004**, 2662; b) L. Benisvy, E. Bill, A. J. Blake, D. Collison, E. S. Davies, C. D. Garner, G. McArdle, E. J. L. McInnes, J. McMaster, S. H. K. Ross, C. Wilson, *Dalton Trans.* **2006**, 258.
- [15] C. Verani, E. Rentschler, T. Weyhermüller, E. Bill, P. Chaudhuri, *J. Chem. Soc., Dalton Trans.* **2000**, 251.
- [16] We tried to simulate this spectrum by considering an axially elongated octahedral Ni^{III} species. The very-low-intensity shoulder at 320 mT was then considered to be associated with the dominant $g = 2.21$ signal. The g_3 value (assimilated to g_{zz}) obtained from the simulation was found much higher (2.09) than those usually reported for such complexes, making the formulation of $[\text{Ni}(\text{L}^3)_2]^+$ as a nickel(III) complex unlikely. The UV/Vis data also argue against this formulation.
- [17] The complexes were found to be insoluble in neat CH₃OH.
- [18] N(CH₃)₂ is strongly electron-donating as reflected by a σ^+ _{Hammett} parameter of -1.17 ; by comparison, the *tert*-butyl and methoxy groups exhibit values of -0.256 and -0.767 , respectively.

Received: April 22, 2008

Published Online: July 14, 2008